

# Edge Errors in Inverse and Wiener Filter Restorations of Motion-Blurred Images and Their Windowing Treatment

HOCK LIM,\* KAH-CHEY TAN,† AND B. T. G. TAN\*

*Laboratory for Image and Signal Processing, National University of Singapore, Kent Ridge, Singapore 0511*

Received May 12, 1989; accepted May 4, 1990

The sensitivity of the inverse filter to noise is often thought to be the reason that inverse filter restorations of motion-blurred images are normally dominated by errors. In this paper, we show that even in the absence of noise, there is a large error component, called the edge error, that arises due to the fact that real images seldom have the periodicity implicitly assumed by discrete Fourier transform operation. An analysis shows that the edge error has a triangular-wave structure with an amplitude proportional to the difference between the average pixel intensity levels of the left and right edges of the image. For the central region of an image, the edge error may be reduced by using Wiener filtering instead of inverse filtering. However, the restored images show reduced resolution as well as ghosting and ringing effects. We also derive mathematically a special window for treatment of the edge error. A significant improvement in the quality of restorations is achieved with the use of this special window. The best restorations are obtained by subjecting the windowed-blurred image to a Wiener filter of large signal-to-noise ratio. © 1991 Academic Press, Inc.

## I. INTRODUCTION

For linear and shift-invariant motion-blurring, the blurred image  $g(x, y)$  may be written as the convolution of the scene  $f(x, y)$  and the point spread function (PSF)  $h(x, y)$ :

$$g(x, y) = \iint_{-\infty}^{\infty} f(\xi, \eta) h(x - \xi, y - \eta) d\xi d\eta + n(x, y), \quad (1)$$

where  $n(x, y)$  represents additive noise. A Fourier transform of Eq. (1) gives

$$G(u, v) = F(u, v)H(u, v) + N(u, v), \quad (2)$$

where  $G(u, v)$ ,  $F(u, v)$ ,  $H(u, v)$ , and  $N(u, v)$  are respectively the transforms of  $g(x, y)$ ,  $f(x, y)$ ,  $h(x, y)$ , and

\* Permanent affiliation: Department of Physics, National University of Singapore, Kent Ridge, Singapore 0511.

† Permanent affiliation: Defence Science Organisation, Science Park, Singapore 0511.

$n(x, y)$ . When the noise term is negligible, a restoration of  $f(x, y)$  may be obtained by an inverse transform of  $G(u, v)/H(u, v)$ . This restoration technique is often called the inverse filter.

The inverse filter, unfortunately, seldom works in practice. Most restored images are completely overwhelmed by errors exhibiting marked periodic structures (e.g., Ref. [1]). These errors are commonly thought to be due to the presence of noise which contributes the error term  $N(u, v)/H(u, v)$ . Near the zeroes of  $H(u, v)$ , the error term becomes very large and thus gives rise to prominent restoration errors. Hence the inverse filter is often dismissed as being too sensitive to noise and hence useless for restoration of real images.

The effect of noise amplification near the zeroes of  $H(u, v)$  can be suppressed by a slight modification of the inverse filter. Instead of the inverse filter  $1/H(u, v)$ , we multiply  $G(u, v)$  by the modified filter function

$$H_1(u, v) = \frac{H^*(u, v)}{H(u, v)H^*(u, v) + \gamma}, \quad (3)$$

where  $H^*(u, v)$  is complex conjugate of  $H(u, v)$  and  $\gamma$  is a constant. When  $\gamma = 0$ , this modified filter reduces to the inverse filter. For finite  $\gamma$ , all the singularities of  $1/H(u, v)$  are converted to zeroes of  $H_1(u, v)$ , and hence the noise amplification effect of the inverse filter is rendered less objectionable. This restoration technique, which is often called the pseudo-inverse filter, can also be derived from the principle of minimum mean-square error. In this case,  $\gamma$  is determined in terms of the signal-to-noise ratio, and the technique is then generally known as the Wiener filter after N. Wiener, who first applied such a principle to the filtering of noisy time series.

The Wiener filter does somewhat improve the restoration. However, it is unfortunately not the most appropriate solution to the problem since, as we shall demonstrate in this paper, random noise is not the main source of the observed restoration errors. In practical inverse or Wiener filtering, only a portion of the complete blurred image  $g(x, y)$  is available and this truncated image is further digitized and subjected to discrete Fourier trans-

forms. In the spectral analysis of time series, the leakage problem due to truncated data was recognized early and many windowing techniques for its treatment have been proposed. A study of the boundary value problem in image restoration by recursive spatial domain filtering was carried out by Woods *et al.* [2]. Li and Wang [3] considered the error due to truncated data in their estimation of the blur extent of a square-pulse PSF.

In this paper, we present a thorough analysis of the restoration errors due to the truncated of image data, which we shall call "edge errors." We first obtain analytic expressions for the edge errors of the inverse filter. This is followed by an examination of the changes in the characteristics of edge errors when Wiener filters are used. We then derive a special window which may be expected to be the most effective for the reduction of edge errors for general images. Restorations obtained using the inverse and Wiener filters, with and without the special window, are finally presented. The better image restorations thus obtained are probably adequate for less demanding applications, but their quality still leaves much to be desired.

Our analysis of edge errors has also led to new techniques for image restoration. In a companion paper, we shall report on two techniques which are capable of almost perfect restoration of a large class of images.

## II. EDGE ERROR

Suppose  $g_i$  is the digitized image of a scene  $f_i$  blurred by a point spread function  $h_i$ :

$$g_i = \sum_{j=0}^{M-1} h_j f_{i-j}, \quad i = 0, 1, \dots, (N-1); N > M. \quad (4)$$

The restored image  $G_u$  may be given by the discrete Fourier transform (DFT) of (4):

$$\begin{aligned} G_u &= \sum_{i=0}^{N-1} g_i W^{iu} = \sum_{i=0}^{N-1} \sum_{j=0}^{M-1} h_j f_{i-j} W^{iu} \\ &= \sum_{j=0}^{M-1} h_j W^{ju} \sum_{i=0}^{N-1} f_i W^{iu} \\ &\quad + \sum_{j=1}^{M-1} \left( h_j W^{ju} \sum_{l=1}^j f_{N-l} W^{-lu} \right) \\ &\quad - \sum_{j=1}^{M-1} \left( h_j W^{ju} \sum_{l=1}^j f_{N-l} W^{(N-l)u} \right), \end{aligned} \quad (5)$$

where  $W = \exp(2\pi\sqrt{-1}/N)$ . Since  $u$  is an integer,  $W^{(N-l)u} = W^{-lu}$ , and (5) thus reduces to

$$G_u = H_u F_u - E_u, \quad (6)$$

where  $F_u$  and  $H_u$  are, respectively, the DFT of  $f_i$  and  $h_i$  (padded with zeroes), and

$$E_u = \sum_{j=1}^{M-1} \left( h_j W^{ju} \sum_{l=1}^j (f_{N-l} - f_{-l}) W^{-lu} \right). \quad (7)$$

In inverse filtering, a restoration is attempted by an inverse DFT of  $G_u/H_u$ :

$$\begin{aligned} \hat{f}_i &= \frac{1}{N} \sum_{u=0}^{N-1} (F_u - E_u/H_u) W^{-iu}, \\ i &= 0, 1, \dots, (N-1). \end{aligned} \quad (8)$$

There is therefore a restoration error given by

$$e_i^{\text{inv}} = f_i - \hat{f}_i = \frac{1}{N} \sum_{u=0}^{N-1} (E_u/H_u) W^{-iu}. \quad (9)$$

Equation (7) shows that the restoration error vanishes when  $f_{N-l} = f_{-l}$ , which is true for images of small objects in a uniform background, or for images artificially blurred with a point spread function that wraps around from one edge of the image to the other.

For real images,  $E_u$  in general does not vanish and a large error in the restoration may be expected. Consider the simple PSF  $h_i = 1/M$ , which is often used as an idealized model for motion-blurring. The zeroes of the corresponding  $H_u$  are at  $u = mN/M$ ,  $m = 1, 2, \dots, (M-1)$ . When  $N$  and  $M$  have a common divisor, some of the zeroes will occur on the computational nodes of the DFT, and direct inverse filtering will fail due to the fatal computational error of division by zero. This computational difficulty may be evaded either by assigning zero values for the affected Fourier components (pseudo-inverse filtering) or by choosing mutually prime  $N$  and  $M$ . Nevertheless, each zero of  $H_u$  may still be expected to give rise to a nearly sinusoidal error component of large amplitude. As all such error components have wavelengths  $M/m$ ,  $m = 1, 2, \dots, (M-1)$ , they add up to form a periodic pattern of period  $M$ . Equation (9) hence shows that even in the absence of random noise, large errors are to be expected in inverse filter restorations.

For the simple PSF under consideration, we may in fact obtain an explicit expression for the edge error. The Fourier transform of  $h_i$  is

$$H_u = \frac{1 - W^{Mu}}{M(1 - W^u)} \quad (10)$$

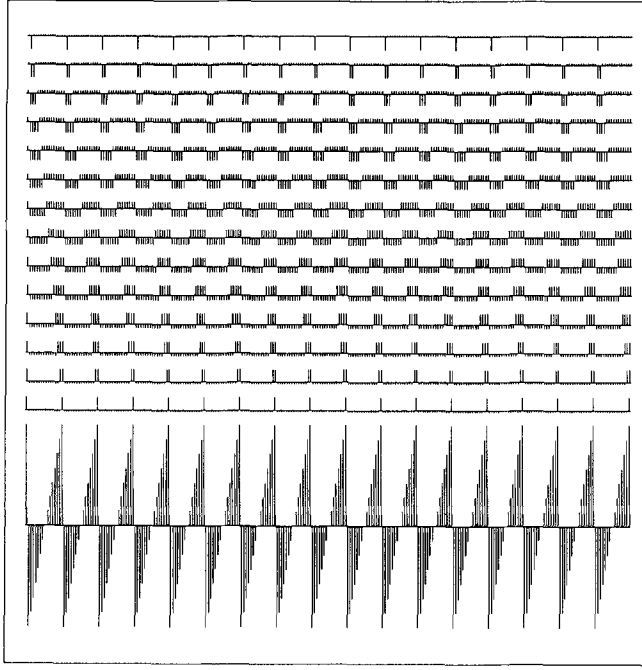


FIG. 1. The 14 plots on the upper half of this figure show consecutively from the top the Green's functions  $G_{l;i}^{\text{inv}}$ ,  $l = 14$  down to 1. The restoration error for the special case  $\phi_l = 1$  for all  $l$  is obtained by summing up all the 14 Green's functions. The result is a triangular wave as shown by the last plot of this figure.

giving for  $E_u$ ,

$$E_u = \sum_{l=1}^{M-1} \phi_l \frac{1 - W^{(M-l)u}}{M(1 - W^u)}, \quad (11)$$

where  $\phi_l = f_{N-l} - f_{-l}$ . The restoration errors are then given by

$$\begin{aligned} e_i^{\text{inv}} &= \sum_{l=1}^{M-1} \phi_l \left( \frac{1}{N} \sum_{u=0}^{N-1} W^{-iu} \frac{1 - W^{(M-l)u}}{1 - W^{Mu}} \right) \\ &= \sum_{l=1}^{M-1} \phi_l G_{l;i}^{\text{inv}}. \end{aligned} \quad (12)$$

Each nonvanishing  $\phi_l$  gives rise to an error pattern over the restored image due to the term enclosed in large parentheses in (12). We denote it by  $G_{l;i}^{\text{inv}}$  as it may be considered as the Green's function for the boundary error term  $\phi_l$ .

The Green's functions  $G_{l;i}^{\text{inv}}$  can be explicitly evaluated as is shown in the Appendix. The upper 14 plots of Fig. 1 show the Green's functions for the case  $M = 15$  and  $N = 17M + 1 = 256$ . We see that  $G_{l;i}^{\text{inv}}$  are square waves centered around zero. The positive phases of the square wave  $G_{l;i}^{\text{inv}}$  are  $l$  pixels long and of a height  $(M-l)/M$ . The

negative phases are  $(M-l)$  pixels long and of a height  $-l/M$ . All the square waves begin with a positive to negative transition from pixel 0 to pixel 1. These Green's functions provide a clear picture of the error patterns expected to arise from the nonperiodicity of the scene  $f_i$ . For instance, if all  $\phi_l = 0$  except  $\phi_1 = f_{255} - f_{-1} = 1$ , the inverse filter restoration will show sharp spikes at pixels 15, 30, . . . , 255. On the other hand, if  $\phi_l = \phi$  (a constant) for all  $l$ , then (12) reduces to

$$\begin{aligned} e_0^{\text{inv}} &= \phi \frac{M-1}{2}; \\ e_i^{\text{inv}} &= \phi \left\{ -\frac{M-1}{2} + ((i-1) \bmod M) \right\}, \\ i &= 1, 2, \dots, (N-1). \end{aligned} \quad (13)$$

The restoration error (13) is shown in the last plot of Fig. 1. Even for a small value of  $\phi = 1$  bit-level, the restored image is marred by a triangular wave of amplitude  $(M-1)$  bit-levels.

### III. EDGE ERROR IN WIENER FILTER

The Wiener filter restoration is given by

$$\hat{f}_i = \frac{1}{N} \sum_{u=0}^{N-1} \frac{W^{-iu} H_u^* G_u}{H_u^* H_u + \gamma}, \quad (14)$$

where  $H_u^*$  is the complex conjugate of  $H_u$ . When  $\gamma$  is zero, the Wiener filter reduces to the inverse filter. For positive, nonzero values of  $\gamma$ , the Wiener filter replaces all the singularities of the inverse filter by zeroes, and hence avoids some of the computational difficulties of the inverse filter. The Wiener filter is also more robust than the inverse filter for restoring noisy images. For these reasons, when a restoration by the inverse filter is not satisfactory, the Wiener filter is often used.

A derivation similar to that for the inverse filter gives

$$\begin{aligned} \hat{f}_i &= \frac{1}{N} \sum_{u=0}^{N-1} \frac{W^{-iu} H_u^* H_u F_u}{H_u^* H_u + \gamma} - \frac{1}{N} \sum_{u=0}^{N-1} \frac{W^{-iu} H_u^* E_u}{H_u^* H_u + \gamma} \\ &= f_i^{\text{wie}} - e_i^{\text{wie}}, \end{aligned} \quad (15)$$

where  $F_u$  and  $E_u$  are as defined in the last section. The second term denoted  $e_i^{\text{wie}}$  on the right-hand side of (15) is the edge-error term. The first term  $f_i^{\text{wie}}$  gives the edge-error-free Wiener filter restoration. Note that the edge-error-free restoration is not a perfect restoration as in the case of the inverse filter.

For the simple PSF  $h_i = 1/M$ , we may substitute (10) and (11) into the edge-error term  $e_i^{\text{wie}}$  and obtain

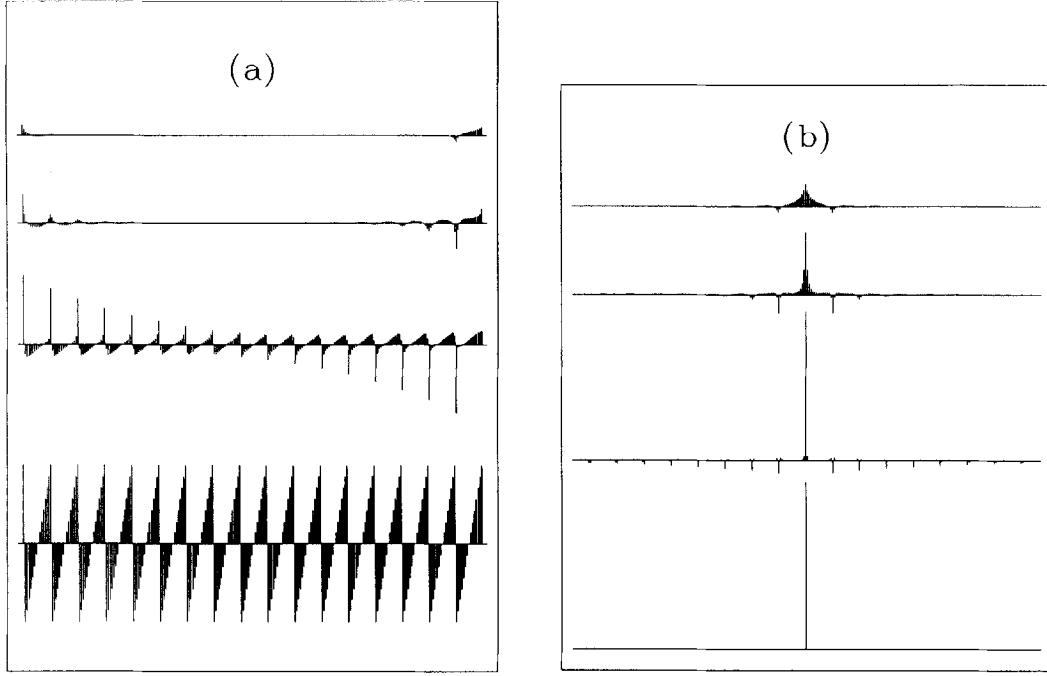


FIG. 2. (a) The edge error of Wiener filters with  $\gamma = 10^{-1}$  (top),  $10^{-2}$ ,  $10^{-4}$ , and  $10^{-8}$  (bottom). Note that for  $\gamma = 10^{-8}$  the edge error is basically the same as that for the inverse filter, whereas for  $\gamma = 10^{-2}$  and  $10^{-1}$ , the edge error is negligible in the central part of the image. (b) The smearing functions  $\sigma_i$  of the Wiener filters of (a). Note that for  $\gamma \geq 10^{-2}$ , there is a negative peak at a distance equal to the blue extent on either side of the main peak at the origin. This indicates the presence of the ghosting effect.

$$e_i^{\text{wie}} = \sum_{l=1}^{M-1} \phi_l \left\{ \frac{1}{N} \sum_{u=0}^{N-1} W^{-iu} \right. \\ \times \left. \frac{(1 - W^{-Mu})(1 - W^{(M-l)u})}{(1 - W^{Mu})(1 - W^{-Mu}) + M^2\gamma(1 - W^u)(1 - W^{-u})} \right\}. \quad (16)$$

To compare the edge error of the Wiener filter with that of the inverse filter, we shall consider the special case of all  $\phi_l = \phi$ . Equation (16) then reduces to

$$e_i^{\text{wie}} = \frac{\phi}{N} \sum_{u=0}^{N-1} W^{-iu} \\ \times \frac{(1 - W^{-Mu})}{(1 - W^{Mu})(1 - W^{-Mu}) + M^2\gamma(1 - W^u)(1 - W^{-u})} \\ \times \left\{ M - 1 + \frac{1 - W^{(M-1)u}}{1 - W^{-u}} \right\}. \quad (17)$$

The edge error as given by (17) is plotted in Fig. 2a for  $\gamma = 10^{-8}$  (bottom),  $\gamma = 10^{-4}$ ,  $\gamma = 10^{-2}$ , and  $\gamma = 10^{-1}$  (top). We see that for  $\gamma = 10^{-8}$ , the edge error is basically the same as that of the inverse filter as shown in Fig. 1. As  $\gamma$  increases, the edge error decreases. For  $\gamma > 10^{-2}$ , the edge error is negligible near the center of the image.

However, a significant edge error remains near the edge. An interesting observation is that while the edge error of the inverse filter is periodic, the edge error of the Wiener filter is not (except for  $\gamma \leq 10^{-8}$ ), and tends to show strong spikes with opposite signs at the two edges of the image.

The reduction of edge error is obtained at a price—an unintentional smearing of the restored image. The edge-error-free restoration may be written as

$$f_i^{\text{wie}} = \frac{1}{N} \sum_{u=0}^{N-1} W^{-iu} \\ \times \frac{(1 - W^{Mu})(1 - W^{-Mu})F_u}{(1 - W^{Mu})(1 - W^{-Mu}) + M^2\gamma(1 - W^u)(1 - W^{-u})}. \quad (18)$$

From the convolution theorem, we see that  $f_i^{\text{wie}}$  is obtained by spreading every pixel of  $f_i$  to a shape  $\sigma_j$  given by

$$\sigma_j(\gamma) = \frac{1}{N} \sum_{u=0}^{N-1} W^{-ju} \\ \times \frac{(1 - W^{Mu})(1 - W^{-Mu})}{(1 - W^{Mu})(1 - W^{-Mu}) + M^2\gamma(1 - W^u)(1 - W^{-u})}. \quad (19)$$

Figure 2b shows  $\sigma_j$  for  $\gamma = 10^{-8}$  (bottom),  $\gamma = 10^{-4}$ ,  $\gamma = 10^{-2}$ , and  $\gamma = 10^{-1}$  (top). When  $\gamma = 10^{-8}$ , there is negligible spreading, consistent with the fact that the corresponding edge error is basically the same as that of the inverse filter. For  $\gamma > 10^{-2}$ , when the edge error near the center of the image is negligible, the spreading is significant. This means that resolution of the restored image will be affected more adversely as the edge error is reduced.

#### IV. REDUCING EDGE ERROR BY WINDOWING

As the edge error arises from the fact that only a finite segment of the whole scene is captured on the image, we now consider the possibility of using windowing techniques to reduce the edge error. Let us consider a general window  $\omega_i$ , with  $\omega_i = 1$  for  $K \leq i \leq (N - L)$ . The shape of the two tapering ends of the window and their lengths  $K, L$  are to be determined for the most effective reduction of edge error. The Fourier transform of the windowed-blurred image is

$$\begin{aligned} \tilde{G}_u &= \sum_{i=0}^{N-1} W^{iu} \omega_i g_i \\ &= \sum_{j=0}^{M-1} h_j W^{ju} \sum_{i=0}^{N-1} f_i W^{iu} \\ &\quad - \sum_{j=0}^{M-1} h_j W^{ju} \left( \sum_{i=0}^{N-1} (1 - \omega_{i+j}) f_i W^{iu} \right) \\ &\quad - \sum_{j=1}^{M-1} h_j W^{ju} \left( \sum_{i=1}^j (f_{N-i} - f_{-i}) W^{-iu} \omega_{j-i} \right) \\ &= H_u F_u - B_u - E_u^{\text{win}}. \end{aligned} \quad (20)$$

The first term by itself will give a perfect restoration. The second term containing the factor  $(1 - \omega_{i+j})$  gives the restoration error due to windowing. In Wiener filtering, the filter error gives rise to a loss of resolution due to smearing. In windowing, the error is additive. The last term gives the edge error, i.e., the error due to the non-vanishing of the terms  $(f_{N-i} - f_{-i})$ .

To facilitate the choice of  $\omega_i$ , let us transform the expressions for  $E_u^{\text{win}}$  and  $B_u$  into summations with respect to the subscript of  $\omega_i$ . The edge-error term becomes

$$E_u^{\text{win}} = \sum_{k=0}^{M-2} W^{ku} \omega_k \left( \sum_{i=1}^{M-k-1} h_{i+k} (f_{N-i} - f_{-i}) \right). \quad (21)$$

The main point to note is that  $E_u^{\text{win}}$  involves only  $\omega_k$  for  $k = 0, 1, \dots, (M - 2)$ . The windowing-error term gives

$$\begin{aligned} B_u &= \sum_{k=0}^{M-2} W^{ku} (1 - \omega_k) \left( \sum_{i=0}^k f_i h_{k-i} \right) \\ &\quad + \sum_{k=M-1}^{K-1} W^{ku} (1 - \omega_k) \left( \sum_{i=k-M+1}^k f_i h_{k-i} \right) \\ &\quad + \sum_{k=N-L+1}^{N-1} W^{ku} (1 - \omega_k) \left( \sum_{i=k-M+1}^k f_i h_{k-i} \right) \\ &\quad + \sum_{k=N}^{N+M-2} W^{ku} (1 - \omega_k) \left( \sum_{i=k-M+1}^{N-1} f_i h_{k-i} \right). \end{aligned} \quad (22)$$

For generality, we assume that  $K, L$  are both larger than  $M$ .

The first two terms of (22) contain  $f_i$  near the left edge of the image while the other two terms contain  $f_i$  near the right edge of the image. The left-edge terms of  $(E_u^{\text{win}} + B_u)$  may then be written as

$$\begin{aligned} &\sum_{k=0}^{M-2} W^{ku} \left\{ (1 - \omega_k) \left( \sum_{i=0}^k f_i h_{k-i} \right) - \omega_k \left( \sum_{i=1}^{M-k-1} f_{-i} h_{i+k} \right) \right\} \\ &\quad + \sum_{k=M-1}^{K-1} W^{ku} (1 - \omega_k) \left( \sum_{i=k-M+1}^k f_i h_{k-i} \right). \end{aligned} \quad (23)$$

The second term of (23) can be eliminated by choosing  $\omega_k = 1$  for  $k = (M - 1), \dots, (K - 1)$ . For given  $h_i$  and  $f_i$ , we may choose  $\omega_k$  such that the first term also vanishes. To obtain a generally applicable window, we must make some assumptions about the image. Except for large blur extent, we may assume that the pixel values around the left edge of the image are rather uniform, i.e.,  $f_i \approx \phi$ . Factoring out the  $f_i$  terms, we see that the first term of (23) will vanish if we choose

$$\omega_k = \sum_{i=0}^k h_i, \quad \text{for } k = 0, 1, \dots, M - 2. \quad (24)$$

The left tapering end of the window is therefore defined in terms of the PSF.

The right-edge terms of  $(E_u^{\text{win}} + B_u)$  are more difficult to eliminate. The last two terms of  $B_u$  given in (22) may be written as

$$\begin{aligned} &\sum_{k=0}^{M-2} W^{ku} (1 - \omega_k) \left( \sum_{i=1}^{M-k-1} f_{N-i} h_{i+k} \right) \\ &\quad + \sum_{k=1}^{L-1} W^{-ku} (1 - \omega_{N-k}) \left( \sum_{i=k}^{M+k-1} f_{N-i} h_{i-k} \right). \end{aligned} \quad (25)$$

In the derivation of the above expression, we have made use of the implicit periodicity of the window, i.e.,  $\omega_{N+k} =$

$\omega_k$ . Combining the above with the right-edge term of  $E_u^{\text{win}}$ , we obtain the right-edge restoration error as

$$\begin{aligned} & \sum_{k=0}^{M-2} W^{ku} \left( \sum_{i=1}^{M-k-1} f_{N-i} h_{i+k} \right) \\ & + \sum_{k=1}^{L-1} W^{-ku} (1 - \omega_{N-k}) \left( \sum_{i=k}^{M+k-1} f_{N-i} h_{i-k} \right). \end{aligned} \quad (26)$$

This error cannot be removed by windowing techniques since irrespective of what  $\omega_{N-k}$  we choose, the two terms of (26) cannot cancel each other as they involve separately positive and negative powers of  $W^u$ . The best course is to choose  $\omega_{N-k}$  so that the effect of this error is the least damaging. The first term of (26) in fact gives us a strong hint of the appropriate measure to be taken.

Consider the sum

$$\begin{aligned} & \sum_{j=0}^{M-1} h_j W^{ju} \sum_{i=N-M+1}^{N-1} f_i W^{iu} \\ & = \sum_{k=0}^{M-2} W^{ku} \left( \sum_{i=1}^{M-k-1} f_{N-i} h_{i+k} \right) + \sum_{k=1}^{M-1} W^{-ku} \left( \sum_{i=k}^{M-1} f_{N-i} h_{i-k} \right). \end{aligned} \quad (27)$$

The first term of (27) is identical to the first term of (26). We may choose  $\omega_{N-k}$  so that the second terms of (26) and (27) also become equal for given  $h_i$  and  $f_i$ . Again assuming that the pixel values  $f_i$  remain uniform near the right edge of the image, the choice will be  $\omega_{N-k} = 1$  for  $k \geq M$  and

$$\omega_{N-k} = \sum_{i=M-k}^{M-1} h_i, \quad \text{for } k = 1, 2, \dots, M-1. \quad (28)$$

The right tapering end of the window is therefore also defined.

We may note that the window as defined in (24) and (28) can be fine-tuned for any given image. If we have approximate values of  $f_i$  in the left and right edges, a special window may be designed using these values. However, such special windows are not applicable to other images.

For the special case of a square-pulse PSF,  $h_i = 1/M$ , the window becomes trapezoidal in shape,

$$\begin{aligned} \omega_k &= \frac{k+1}{M}, \quad \text{for } k = 0, 1, \dots, M-2, \\ \omega_k &= \frac{N-k}{M}, \quad \text{for } k = N-M+1, \dots, N-1, \\ \omega_k &= 1, \quad \text{otherwise.} \end{aligned} \quad (29)$$

Trapezoidal windows have also been proposed by Chen [4]. However, our derivation here provides a theoretical basis for the trapezoidal window and resolves issues such as the proper width for the tapering ends.

Applying the window as defined by (24) and (28), we have

$$\begin{aligned} \tilde{G}_u &= \sum_{j=0}^{M-1} h_j W^{ju} \left( \sum_{i=0}^{N-M} f_i W^{iu} \right) \\ & - \sum_{k=0}^{M-2} W^{ku} \left\{ \sum_{l=k+1}^{M-1} h_l \sum_{i=0}^k f_i h^{k-i} - \sum_{l=0}^k h_{k-l} \sum_{i=0}^{M-k-1} f_{-i} h_{i+k} \right\} \\ & - \sum_{k=1}^{M-1} W^{-ku} \left\{ \sum_{l=0}^{M-k-1} h_l \sum_{i=k}^{M+k-1} f_{N-i} h_{i-k} - \sum_{i=k}^{M-1} f_{N-i} h_{i-k} \right\}. \end{aligned} \quad (30)$$

As expected, when  $f_i$  remains constant around the left edge and the right edge separately, the last two terms of (30) vanish, and the restored image is given by the first term. Note that the second summation of the first term is from  $i = 0$  to  $i = (N - M)$ . This implies that the restored image  $\hat{f}_i$  is perfect (i.e.,  $\hat{f}_i = f_i$ ) except that a band of width  $(M - 1)$  is completely blanked out ( $\hat{f}_{N-M+1} = \hat{f}_{N-M+2} = \dots = \hat{f}_{N-1} = 0$ ).

For a general image,  $f_i$  cannot be assumed to be constant around the edges. Equation (30) then implies that there will be an edge error in the restoration apart from the blanking of the  $(M - 1)$  rightmost pixels. However, as the edge error is now proportional to the degree of non-uniformity of  $f_i$  at the left and right edges taken separately instead of the differences  $(f_{N-i} - f_i)$ , a considerable reduction of the edge error may be expected.

## V. IMAGES RESTORED BY THE VARIOUS METHODS

In this section, we present some images restored by the various methods discussed. In Figs. 3a–3j, we have used a monochrome image of the book cover design of the textbook on image restoration by Andrews and Hunt [5]. Figure 3a is the original image of  $497 \times 512$  resolution. Figure 3b is the blurred image obtained with a square-pulse PSF of 16-point blur extent. Figure 3c is the inverse filter restoration which is completely dominated by edge error. Figure 3d is the restoration obtained by inverse filtering the data after application of the trapezoid window (29). The results are still very poor.

Figures 3e–3g show, respectively, the Wiener filter restorations with  $\gamma = 10^{-4}, 10^{-2}$ , and  $10^{-1}$ . With increasing value of  $\gamma$ , the edge error decreases, but the restorations lose resolution. A “ghosting” (or ringing) effect becomes noticeable for  $\gamma \geq 10^{-2}$ . Such a ghosting effect is consistent with Fig. 2b, which shows that for larger  $\gamma$



**FIG. 3.** Restoration of an image by the various restoration methods. (a) The original scene. (b) The blurred image (square-pulse PSF). (c) The inverse filter restoration. (d) The trapezoid window/inverse filter restoration. (e) The Wiener filter restoration with  $\gamma = 10^{-4}$ . (f) Same as (e) but for  $\gamma = 10^{-2}$ . (g) Same as (e) but for  $\gamma = 10^{-1}$ . (h) The trapezoid window/Wiener filter ( $\gamma = 10^{-4}$ ) restoration. (i) Same as (h) but for  $\gamma = 10^{-2}$ . (j) Same as (i) but for  $\gamma = 10^{-1}$ .

values, there tends to be a negative peak at one blur-extent distance on either side of the main peak at the origin.

Figures 3h–3j show the results of Wiener filtering ( $\gamma = 10^{-4}, 10^{-2}, 10^{-1}$ , respectively) after applying the trapezoid window to the blurred image. The edge error is reasonably well controlled and a significant improvement in

image quality over the corresponding Figs. 3e–3g is obtained.

From the above illustrations, we may conclude that our mathematical analyses presented in the earlier sections have correctly identified the edge error as the main source of error in the inverse and Wiener filter restorations. The trapezoid window we have derived is also ef-



FIG. 3—Continued

fective in improving the quality of the restorations. The best results appear to be obtained by applying a Wiener filter with  $10^{-4} \leq \gamma \leq 10^{-2}$  to data treated with the trapezoid window. However, we note that even with the help of the trapezoid window, none of the restorations appear to be satisfactory for the most demanding applications.

## VI. SUMMARY AND CONCLUSIONS

Large errors are often observed in inverse filter restoration of images. Such errors are commonly attributed to

noise which is amplified by the singularities of the inverse filter. In view of the sensitivity of the inverse filter to noise, it has been dismissed as impractical for the restoration of real images.

In the literature, three different approaches seem to have been taken in reducing the restoration errors: (1) replacing the inverse filter with Wiener filters, (2) windowing the blurred image before restoration, and (3) working in the spatial domain rather than in the Fourier transform domain (e.g., Ref. [6]).

In this paper, we have addressed the first two ap-

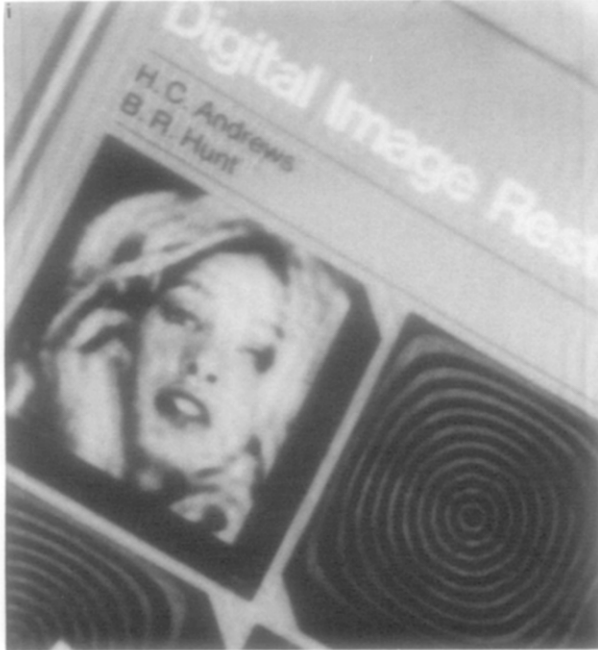


FIG. 3—Continued

proaches. We first presented an analysis of the edge error in inverse and Wiener filter restorations of motion-blurred images. The application of the discrete convolution theorem implicitly requires that the data be periodic. As true images are rarely periodic over their width, a direct application of the convolution theorem as in the inverse filter leads to edge errors. Such edge errors are generally of overwhelming amplitudes and appear in the form of periodic bands, with the pixel intensity varying from extreme white to extreme black within a period.

The edge error can be reduced, especially near the center part of the image, by using Wiener filters instead of the inverse filter. By increasing the filter parameter ( $\gamma$ ), the edge error becomes less prominent, but the resolution of the restored images also becomes smeared. A ghosting effect becomes clearly visible for  $\gamma \geq 0.01$ .

A further improvement in the quality of the restoration is obtained with the use of windowing. From the consideration of edge-error reduction, we derived a window which is expressible in terms of the PSF. With the window, Wiener filters with  $\gamma$  ranging from 0.0001 to 0.01 seem to yield acceptable restorations.

It appears that even with the help of appropriate windowing, traditional restoration techniques with the inverse and Wiener filters are still not capable of restoring images to the quality obtained with spatial-domain methods such as that of Sondhi [6]. It however does not necessarily follow that spatial-domain methods are superior to Fourier-transform-domain methods. The expressions for the edge error which we have obtained can in fact be used for the design of new Fourier-transform-domain restoration methods. In a companion paper, we shall propose

some new techniques which are capable of near-perfect restoration of a large class of noise-free images.

#### APPENDIX: EVALUATION OF $G_{i,i}^{\text{inv}}$

We start with the identity

$$\begin{aligned} & \frac{1}{N} \sum_{u=0}^{N-1} W^{-iu} \frac{1 - W^{(M-l)u}}{1 - W^u} \\ &= \frac{1}{N} \sum_{u=0}^{N-1} W^{-iu} (1 + W^u + W^{2u} + \dots + W^{(M-l-1)u}) \\ &= \begin{cases} 1, & \text{for } 0 \leq i \leq (M-l-1); \\ 0, & \text{for } (M-l) \leq i \leq (N-1). \end{cases} \end{aligned} \quad (\text{A1})$$

Equation (A1) implies

$$\begin{aligned} & \frac{1}{N} \sum_{u=0}^{N-1} W^{-iu} \frac{1 - W^{(M-l)u}}{1 - W^{Mu}} \\ & \times (1 + W^u + W^{2u} + \dots + W^{(M-1)u}) \\ &= \begin{cases} 1, & \text{for } 0 \leq i \leq (M-l-1); \\ 0, & \text{for } (M-l) \leq i \leq (N-1). \end{cases} \end{aligned} \quad (\text{A2})$$

Exploiting the periodicity of  $W^{-iu}$ , we obtain from (A2)  $N$  equations relating the  $G_i^{\text{inv}}$ :

$$\mathbf{Av} = \mathbf{c}, \quad (\text{A3})$$

where  $\mathbf{v}$  is the vector ( $N \times 1$  matrix)  $[G_{l,0}^{\text{inv}}, G_{l,1}^{\text{inv}}, \dots, G_{l,N-1}^{\text{inv}}]^T$ ,  $\mathbf{c}$  the constant vector with the first  $(M - l)$  elements equal to 1 and the remaining elements equal to 0, and  $\mathbf{A}$  a circulant matrix. The first row of  $\mathbf{A}$  consists of elements  $a_{1,1} = 1$ ,  $a_{1,2} = \dots = a_{1,N-M} = 0$ , and  $a_{1,N-M+1} = \dots = a_{1,N} = 1$ . Subsequent rows of  $\mathbf{A}$  are obtained by rolling the first row successively to the right.

When  $N = mM + 1$ ,  $m$  an integer, an analysis of (A3) shows that the elements  $G_{l,i}^{\text{inv}}$  are divided into two classes; in each class the elements  $G_{l,i}^{\text{inv}}$  are all equal to a constant value:

$$G_{l,0}^{\text{inv}} = (M - l)/M,$$

$$G_{l,i}^{\text{inv}} = -l/M$$

for  $0 \leq \{(i - 1) \bmod M\} \leq (M - l - 1)$ , (A4)

$$G_{l,i}^{\text{inv}} = (M - l)/M$$

for  $(M - l) \leq \{(i - 1) \bmod M\} \leq (M - 1)$ . (A4)

Solutions (A4) are square waves. A specific example is shown in Fig. 1.

## REFERENCES

1. H. Shvayster and S. Peleg, Inversion of picture operators, *Pattern Recognit. Lett.* **5**, 1987, 49–61.
2. J. W. Woods, J. Biemond, and A. M. Tekalp, Boundary value problem in image restoration, in *Proceedings, ICASSP 85, Tampa, Florida*, pp. 692–695.
3. Han Li and Yenping Wang, A new model of motion blurred images and estimation of its parameter, in *Proceedings, ICASSP 86, Tokyo*, pp. 2447–2450.
4. Chen-Tie Chen, An investigation to reduce artifacts in image restoration, in *Proceedings, Conf. Info. Sciences and Systems, March 1987*.
5. H. C. Andrews and B. R. Hunt, *Digital Image Restoration*, Prentice-Hall, Englewood Cliffs, NJ, 1977.
6. M. M. Sonndhi, Image restoration: The removal of spatially invariant degradations, *Proc. IEEE* **60**, No. 7, 1972, 828–842.